Fully Convolutional Pixel Adaptive Image Denoiser

Sungmin Cha[1] and Taesup Moon[1,2]
[1]Department of Electrical and Computer Engineering, [2] Department of Artificial Intelligence
Sungkyunkwan University, Suwon, Korea 16419
{csm9493,tsmoon}@skku.edu

Abstract

We propose a new image denoising algorithm, dubbed as Fully Convolutional Adaptive Image DEnoiser (FC-AIDE), that can learn from an offline supervised training set with a fully convolutional neural network as well as adaptively fine-tune the supervised model for each given noisy image. We significantly extend the framework of the recently proposed Neural AIDE, which formulates the denoiser to be context-based pixelwise mappings and utilizes the unbiased estimator of MSE for such denoisers. The two main contributions we make are; 1) implementing a novel fully convolutional architecture that boosts the base supervised model, and 2) introducing regularization methods for the adaptive fine-tuning such that a stronger and more robust adaptivity can be attained. As a result, FC-AIDE is shown to possess many desirable features; it outperforms the recent CNN-based state-of-the-art denoisers on all of the benchmark datasets we tested, and gets particularly strong for various challenging scenarios, e.g., with mismatched image/noise characteristics or with scarce supervised training data. The source code our algorithm is available at https://github.com/csm9493/FC-AIDE-Keras.

1. Introduction

Image denoising, which tries to recover a clean image from its noisy observation, is one of the oldest and most prevalent problems in image processing and low-level computer vision. While numerous algorithms have been proposed over the past few decades, *e.g.*, [8, 2, 7, 11, 9, 21], the current throne-holders in terms of the average denoising performance are convolutional neural network (CNN)-based methods [38, 22, 31].

The main idea behind the CNN-based method is to treat denoising as a supervised regression problem; namely, first collect numerous clean-noisy image pairs as a supervised training set, then learn a regression function that maps the noisy image to the clean image. Such approach is relatively simple since it does not require any complex priors on the underlying clean images and let CNN figure out to learn the correct mapping from the vast training data. Despite the conceptual simplicity, several recent variations of the CNN-based denoisers using residual learning [38], skip-connections [22], and densely connected structure [31] have achieved impressive state-of-the-art performances.

However, we stress that one apparent drawback exists in above methods; namely, they are solely based on offline batch training of CNN, hence, lack adaptivity to the given noisy image subject to denoising. Such absence of adaptivity, which is typically possessed in other prior or optimization-based methods, *e.g.*, [8, 2, 7, 11, 9, 21], can seriously deteriorate the denoising performance of the CNN-based methods in multiple practical scenarios in which various mismatches exist between the training data and the given noisy image. One category of such mismatch is the *image mismatch*, in which the image characteristics of the given noisy image are not well represented in the offline training set. The other category is *noise mismatch*, in which the noise level or the distribution for the given noisy image is different from what the CNN has been trained for. Above drawbacks can be partially addressed by building a composite training set with multiple noise and image characteristics, *e.g.*, the so-called blind training [16, 38], but the limitation of such approach is evident since building large-scale supervised training set that sufficiently contains all the variations is not always possible in many applications.

To that end, we propose a new CNN-based denoising algorithm that can learn from an offline supervised training set, like other recent state-of-the-arts, as well as *adaptively* fine-tune the denoiser for each given noisy image, like other prior or optimization based methods. The main vehicle for devising our algorithm, dubbed as FC-AIDE (Fully Convolutional Adaptive Image DEnoiser), is the framework recently proposed in [4]. Namely, we formulate the denoiser to be context-based pixelwise mappings and obtain the SURE (Stein's Unbiased Risk Estimator)[30]-like estimated losses of the mean-squared errors (MSE) for the mappings. Then, the specific mapping for each pixel is learned with a neural network first by supervised training

using the MSE, then by adaptively fine-tuning the network with the given noisy image using the devised estimated loss. While following this framework, we significantly improve the original Neural AIDE (N-AIDE) [4] by making the following two main contributions. Firstly, we devise a novel fully *convolutional* architecture instead of the simple fully-connected structure of N-AIDE so that the performance of the base supervised model can be boosted. Moreover, unlike [4], which only employed the pixelwise affine mappings, we also consider *quadratic* mappings as well. Secondly, we introduce two regularization methods for the adaptive fine-tuning step: data augmentation and ℓ_2-SP (Starting Point) regularization [18]. While these techniques are well-known for general supervised learning setting, we utilize them such that the fine-tuned model does not *overfit* to the estimated loss and generalize well to the MSE, leading to larger and more robust improvements of the fine-tuning step. With above two contributions, we show that FC-AIDE significantly surpasses the performance of the original N-AIDE as well as the CNN-based state-of-the-arts in several widely used benchmark datasets. Moreover, we highlight the effectiveness of the adaptivity of our algorithm in multiple challenging scenarios, e.g., with image/noise mismatches or with scarce supervised training data.

2. Related Work

There are vast number of literature on image denoising, among which the most relevant ones are elaborated here.

Deep learning based denoisers Following the pioneering work [14, 3, 36], recent deep learning based methods [38, 22, 31] apply variations of CNN within the supervised regression framework and significantly surpassed the previous state-of-the-arts in terms of the denoising PSNR. More recently, [6, 19] explicitly designed a non-local filtering process within the CNN framework and showed some more improvements with the cost of increased running time. For the cases with lack of clean data in the training data, [17] proposed a method that trains the CNN-based denoiser only with the noisy data, provided that two independent noise realizations for an image are available.

Adaptive denoisers In contrast to above CNN-based state-of-the-arts, which freeze the model parameters once the training is done, there are many approaches that can learn a denoising function adaptively from the given noisy image, despite some PSNR shortcomings. Some of the classical methods are the filtering approach [2, 7], optimization-based methods with sparsity or low-rank assumptions [9, 21, 11], Wavelet transform-based [8], and effective prior-based methods [39]. More recently, several work proposed to implement deep learning-based priors or regularizers, such as [32, 37, 20], but their PSNR results still could not compete with the supervised trained CNN-based denoisers.

Another branch of adaptive denoising is the universal denoising framework [35], in which no prior or probabilistic assumptions on the clean image are made, and only the noise is treated as random variables. The original *discrete* denoising setting of [35] was extended to grayscale image denoising in [26, 28], but the performance was not very satisfactory. A related approach is the SURE-based estimators that minimize the unbiased estimates of MSE, *e.g.*, [8, 10], but they typically select only a few tunable hyperparameters for the minimization. In contrast, using the unbiased estimate as an empirical risk in the empirical risk minimization (ERM) framework to learn an entire parametric model was first proposed in [25, 4] for denoising. To the best of the authors' knowledge, [4] was the first deep learning-based method that has both the supervised learning capability and the adaptivity. [29] also proposed to use SURE and Monte-Carlo approximation for training a CNN-based denoiser, but the performance fell short of the supervised trained CNNs.

Blind denoisers Most of above methods assume that the noise model and variance are known *a priori*. To alleviate such strong assumption, the supervised, *blindly* trained CNN models [16, 38] were proposed, and they show quite strong performance due to CNN's inherent robustness. But, those models also lack adaptivity, *i.e.*, they cannot adapt to the specific noise realizations of the given noisy image.

3. Problem Setting and Preliminaries

3.1. Notations and assumptions

We generally follow [4], but introduce more compact notations. First, we denote $\mathbf{x} \in \mathbb{R}^n$ as the clean image and $\mathbf{Z} \in \mathbb{R}^n$ as its additive noise-corrupted version, namely, $\mathbf{Z} = \mathbf{x} + \mathbf{N}$. We make the following assumptions on $\mathbf{N}$;

- $\mathbb{E}(\mathbf{N}) = \mathbf{0}$ and $\mathrm{Cov}(\mathbf{N}) = \sigma^2 \mathbf{I}_{n\times n}$.
- Each noise component, N_i, is independent and has a symmetric distribution.re

Note we do not necessarily assume the noise is identically distributed or Gaussian. Moreover, as in universal denoising, we treat the clean $\mathbf{x}$ as an individual image without any prior or probabilistic model and only treat $\mathbf{Z}$ as random, which is reflected in the upper case notation.

A denoiser is generally denoted by $\hat{\mathbf{X}}(\mathbf{Z}) \in \mathbb{R}^n$, of which the i-th reconstruction, $\hat{X}_i(\mathbf{Z})$, is a function of the entire noisy image $\mathbf{Z}$. The standard loss function to measure the denoising quality is MSE, denoted by

$$\mathbf{\Lambda}_n(\mathbf{x}, \hat{\mathbf{X}}(\mathbf{Z})) \triangleq \frac{1}{n}\|\mathbf{x} - \hat{\mathbf{X}}(\mathbf{Z})\|_2^2. \tag{1}$$

3.2. N-AIDE and the unbiased estimator

While $\hat{X}_i(\mathbf{Z})$ can be any general function, we can consider a d-th order polynomial function form for the denoiser,

$$\hat{X}_i(\mathbf{Z}) = \sum_{m=0}^{d} a_m(\mathbf{Z}^{-i}) Z_i^m, \quad i = 1, \ldots, n, \tag{2}$$

in which $\mathbf{Z}^{-i}$ stands for the entire noisy image *except* for Z_i, the i-th pixel, and $a_m(\mathbf{Z}^{-i})$ stands for the coefficient for the m-th order term of Z_i. Note [4] focused on the case $d = 1$, and in this paper, we consider the case $d = 2$ as well. Note $\hat{X}_i(\mathbf{Z})$ can be a highly nonlinear function of $\mathbf{Z}$ since $a_m(\cdot)$'s can be any nonlinear functions of $\mathbf{Z}$.

For (2) with $d \in \{1, 2\}$, by denoting $a_m(\mathbf{Z}^{-i})$ as $a_{m,i}$ for brevity, we can define an unbiased estimator of (1) as

$$\mathbf{L}_n(\mathbf{Z}, \hat{\mathbf{X}}(\mathbf{Z}); \sigma^2) \tag{3}$$
$$\triangleq \frac{1}{n}\|\mathbf{Z} - \hat{\mathbf{X}}(\mathbf{Z})\|_2^2 + \frac{\sigma^2}{n}\sum_{i=1}^{n}\Big[\sum_{m=1}^{d} 2^m a_{m,i} Z_i^{m-1} - 1\Big].$$

Note (3) does *not* depend on $\mathbf{x}$, and the following lemma states the unbiasedness of (3).

Lemma 1 *For any* $\mathbf{N}$ *with above assumptions and* $\hat{\mathbf{X}}(\mathbf{Z})$ *that has the form (2) with* $d \in \{1, 2\}$,

$$\mathbb{E}\mathbf{L}_n(\mathbf{Z}, \hat{\mathbf{X}}(\mathbf{Z}); \sigma^2) = \mathbb{E}\mathbf{\Lambda}_n(\mathbf{x}, \hat{\mathbf{X}}(\mathbf{Z})). \tag{4}$$

Moreover, when $\mathbf{N}$ *is white Gaussian, (3) coincides with the SURE [30].*

Remark: The proof of the lemma is given in the Supplementary Material, and it critically relies on the specific polynomial form of the denoiser in (2). Namely, it exploits the fact that $\mathbf{x}$ is an individual image and $\{a_{m,i}\}$'s are conditionally independent of Z_i given $\mathbf{Z}^{-i}$. Note (4) holds for *any* additive white noise with symmetric distribution, not necessarily only for Gaussian. (The symmetry condition is needed only for $d = 2$ case.) Such property enables the strong adaptivity of our algorithm as shown below.

N-AIDE in [4] can be denoted by $\hat{\mathbf{X}}_{\texttt{N-AIDE}}(\mathbf{w}, \mathbf{Z}) \in \mathbb{R}^n$, of which $\hat{X}_i(\mathbf{w}, \mathbf{Z})$ has the form (2) with $d = 1$ and

$$a_{m,i} = a_m(\mathbf{Z}^{-i}) \triangleq a_m(\mathbf{w}, \mathbf{C}_{k\times k}^{-i}) \tag{5}$$

for $m = 0, 1$. In (5), $\mathbf{C}_{k\times k}^{-i}$ stands for the two-dimensional noisy $k \times k$ patch surrounding Z_i, but *without* Z_i, and $\{a_m(\mathbf{w}, \mathbf{C}_{k\times k}^{-i})\}_{m=0,1}$ are the outputs of a fully-connected neural network with parameter $\mathbf{w}$ that takes $\mathbf{C}_{k\times k}^{-i}$ as input. Note $\mathbf{w}$ does not depend on location i, hence, the denoising by N-AIDE is done in a sliding-window fashion; that is, the neural network subsequently takes $\mathbf{C}_{k\times k}^{-i}$ as an input and generates the affine mapping coefficients for Z_i to obtain the reconstruction for each pixel i.

As mentioned in the Introduction, the training of the network parameter $\mathbf{w}$ for N-AIDE was done in two stages. Firstly, for supervised training, a separate training set $\mathcal{D} = \{(\tilde{x}_i, \tilde{\mathbf{C}}_{i,k\times k})\}_{i=1}^N$ based on many clean-noisy image pairs, $(\tilde{\mathbf{x}}, \tilde{\mathbf{Z}})$, is collected. Here, $\tilde{\mathbf{C}}_{i,k\times k}$ denote the full $k \times k$ patch *including* the center pixel $\tilde{Z}_i$. Then, a supervised model, $\tilde{\mathbf{w}}_{\text{sup}}$, the network parameters for a denoiser $\hat{\mathbf{X}}(\mathbf{w}, \tilde{\mathbf{Z}})$ that has the form of (5), is learned by minimizing the MSE on $\mathcal{D}$, *i.e.*, $\mathbf{\Lambda}_N(\tilde{\mathbf{x}}, \hat{\mathbf{X}}(\mathbf{w}, \tilde{\mathbf{Z}}))$. Secondly, for a given noisy image $\mathbf{Z}$ subject to denoising, the adaptive fine-tuning is carried out by further minimizing the estimated loss $\mathbf{L}_n(\mathbf{Z}, \hat{\mathbf{X}}(\mathbf{w}, \mathbf{Z}); \sigma^2)$ starting from $\tilde{\mathbf{w}}_{\text{sup}}$. The fine-tuned model parameters, denoted by $\hat{\mathbf{w}}_{\texttt{N-AIDE}}$, are then used to obtain the mapping for each pixel i as in (2) using (5), and $\mathbf{Z}$ is pixelwise denoised with those affine mappings. Note maintaining the denoiser form (2), and not the ordinary form of the direct mapping from the full noisy patch to the clean patch, is a key for enabling the fine-tuning.

4. FC-AIDE

4.1. Fully convolutional QED architecture

Limitation of N-AIDE While the performance of N-AIDE [4] was encouraging, the final denoising performance was slightly worse (about $\sim$ 0.15dB) than that of DnCNN-S [38], which applies the ordinary supervised learning with CNN and residual learning. We believe such performance difference is primarily due to the simple fully-connected architecture used in [4, Figure 1] as opposed to the fully convolutional architectures in recent work, *e.g.*, [38, 22, 31].

In order to utilize the convolutional architecture for the N-AIDE framework, we first make an observation that the sliding-window nature of N-AIDE is indeed a convolution operation. Namely, once we use the masked $k \times k$ convolution filters with a *hole* (*i.e.*, the center set to 0) in the first layer and use the ordinary 1×1 filters for the higher layers, the resulting fully convolutional network operating on a noisy image becomes equivalent to the fully-connected network of N-AIDE working in a sliding-window fashion. Note with the standard zero-padding, the output of the network has the same size as the input image and consists of two channels, one for each of $\{a_{m,i}\}_{m=0}^1$ for all location i.

From this observation, we identify a critical constraint for implementing a fully convolutional architecture for the denoisers that have the form (2); that is, the i-th pixel of *any* feature maps at *any* layer should *not* depend on Z_i, and the filters at the output layer must keep the 1×1 structure. Such property is necessary for maintaining the conditional independence between $\{a_{m,i}\}_{m=0}^d$ and Z_i given $\mathbf{Z}^{-i}$, which is critical for the unbiasedness of $\mathbf{L}_n(\mathbf{Z}, \hat{\mathbf{X}}(\mathbf{Z}); \sigma^2)$ shown in Lemma 1. Due to this constraint, we can see that simply applying the vanilla convolutional architecture as in [38] is not feasible for extending N-AIDE beyond the 1×1 structure.

Overall architecture of FC-AIDE To address above limitation of N-AIDE, we now propose FC-AIDE, denoted as $\hat{\mathbf{X}}_{\texttt{FC-AIDE}}(\mathbf{w}, \mathbf{Z})$, that has the fully convolutional architecture and gradually increases the receptive fields as the layer increases, while satisfying above mentioned constraint. Moreover, we also extend to employ the *quadratic*

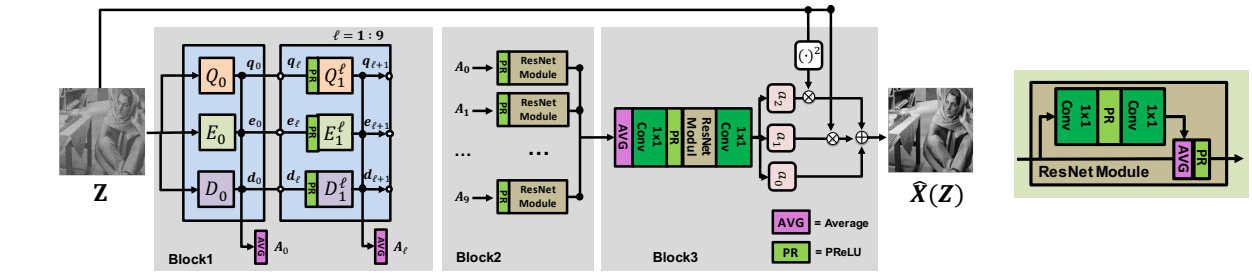

(a) Overall architecture of FC-AIDE (b) ResNet Module

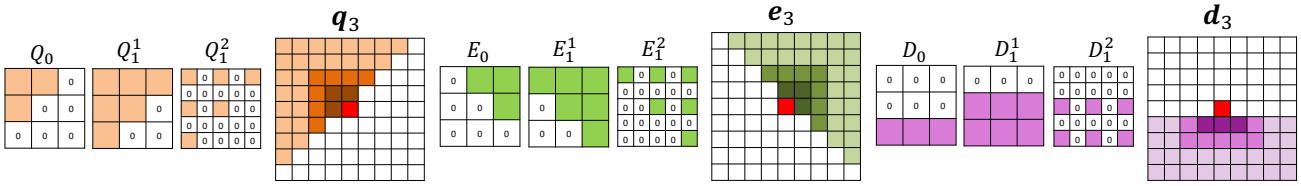

(c) Q-filters and the receptive field at layer 3 (d) E-filters and the receptive field at layer 3 (e) D-filters and the receptive field at layer 3

Figure 1. Overall architecture of FC-AIDE and descriptions of the QED filter classes.

pixelwise mappings, *i.e.*, use $d = 2$ for (2), to take into account of more nonlinearity in learning a denoiser. Namely, the i-th reconstruction of FC-AIDE becomes

$$\hat{X}_{i,\texttt{FC-AIDE}}\,(\mathbf{w}, \mathbf{Z}) = a_{2,i} Z_i^2 + a_{1,i} Z_i + a_{0,i}, \qquad (6)$$

in which $\{a_{m,i}\}$'s are defined as (5) for $m = 0, 1, 2$.

Figure 1(a) summarizes the overall architecture of our FC-AIDE. In Block 1, the three types of *masked* dilated convolution filters, dubbed as Q-, E-, and D-filters, are stacked up to 10 layers, in which the specific filter forms for each class (up to layer 3) are depicted in Figure 1(c)∼1(e), respectively. Note, as shown in Figure 1(a), the filters in each filter class is separately applied on its own input feature map, denoted as $\boldsymbol{q}_\ell$, $\boldsymbol{e}_\ell$, and $\boldsymbol{d}_\ell$ for $\ell = 0, \ldots, 9$. Due to the specific masked structure of the filters, the receptive field of each filter class for the i-th pixel in a feature map (colored in red in Figure 1(c)∼1(e)) gradually grows as the number of layers increases, while not containing Z_i. The example receptive fields at layer 3, i.e., $\boldsymbol{q}_3$, $\boldsymbol{e}_3$, and $\boldsymbol{d}_3$, for the red pixel are shown in Figure 1(c)∼1(e). Now, since the receptive fields for the three filter classes cover complementary halfspaces of the input image, combining the three types of feature maps at layer ℓ (*e.g.*, averaging) generates a feature map A_ℓ, of which the i-th pixel depends on $\mathbf{C}_{k\times k}^{-i}$ with $k = 3 + \ell(\ell - 1)$ for $\ell \geq 1$. Note due to the *dilated* filters for $\ell \geq 2$, the receptive fields grow quickly with the number of layers, while saving the number of parameters.

Once the averaged feature maps $A_0, \ldots, A_9$ are generated from each layer, in Block 2 of Figure 1(a), the PReLU [12] activation and ResNet Module, shown in Figure 1(b), are applied to carry out additional nonlinear transformations of the feature maps. Finally, in Block 3, the feature maps from all layers (with different receptive fields) are averaged, 1x1 Conv with PReLU and one more ResNet Module is applied, and the three 1×1 convolution filters are applied to generate the pixelwise coefficients, *i.e.*, $\{a_{m,i}\}$'s for $m = 0, 1, 2$ and for all i. Note our overall architecture is indeed fully convolutional, and since all the filters in Block 2 and 3 are 1×1, the critical conditional independence constraint is satisfied.

We used 64 filters for all convolution layers in the model. The resulting number of parameters was about 820K, which is about 63% smaller than that of N-AIDE in [4]. However, thanks to the dilated filters, the receptive field size at the final layer was 93×93, much larger than N-AIDE. The training of FC-AIDE is done similarly as the description given in Section 3.2 for N-AIDE, except for the additional regularization methods for fine-tuning given in the next section.

Remark 1: The conditional independence constraint similar to ours has also appeared in [33], in which "one-sided" contexts for sequentially generating images was considered. In contrast, FC-AIDE needs to utilize the whole "double-sided" context, $\mathbf{C}_{k\times k}^{-i}$, for generating pixelwise mappings.

Remark 2: We note that filter classes other than our QED filters can also cover complementary halfspaces around Z_i, *e.g.*, 4 filter classes that cover 4 perpendicular halfspaces surrounding a pixel. However, using three filter classes (as our QED filters or their 45°-rotated versions) turns out to be the most parameter-efficient choice.

4.2. Regularization for adaptive fine-tuning

The fully-convolutional QED architecture in Section 4.1 expands the function approximation capability and improves the base supervised model benefitting from the abun-

dant supervised training data. For the adaptive fine-tuning, however, the only "training data" is the given noisy image $\mathbf{Z}$, *i.e.*, the test data, hence, is prone to *overfitting* as the complexity of model increases. Namely, while the estimated loss (3), based on $\mathbf{Z}$, is minimized during fine-tuning, the true MSE (1), based on both $\mathbf{x}$ and $\mathbf{Z}$, may not be minimized as much. Note the notion of overfitting and generalization for the fine-tuning is different from the ordinary one; *i.e.*, while the ordinary supervised learning cares about the performance with respect to the *unseen* test data, our fine-tuning cares about the performance with respect to the *unseen* clean data. In order to address this overfitting issue, we implement two regularization schemes for adaptive fine-tuning: data augmentation and ℓ_2-SP regularization [18].

First, for data augmentation, we consider $\mathcal{A}(\mathbf{Z})$, which is the augmented dataset that consists of $\mathbf{Z}$ and its horizotally, vertically, and both horizontally and vertically flipped versions. Then, we define $\mathbf{L}_n^{\text{aug}}(\cdot)$ as the average of the estimated losses on $\mathcal{A}(\mathbf{Z})$, *i.e.*,

$$\mathbf{L}_n^{\text{aug}}(\mathbf{Z}, \mathbf{w}; \sigma^2) \triangleq \frac{1}{4} \sum_{\mathbf{Z}^{(j)} \in \mathcal{A}(\mathbf{Z})} \mathbf{L}_n\big(\mathbf{Z}^{(j)}, \hat{\mathbf{X}}(\mathbf{w}, \mathbf{Z}^{(j)}); \sigma^2\big).$$

Then, the ℓ_2-SP regularization adds the squared ℓ_2-norm penalty on the deviation from the supervised trained FC-AIDE model, $\tilde{\mathbf{w}}_{\text{sup}}$, and modify the objective function for fine-tuning as

$$\mathbf{L}_n^{\text{aug}}(\mathbf{Z}, \mathbf{w}; \sigma^2) + \lambda \|\mathbf{w} - \tilde{\mathbf{w}}_{\text{sup}}\|_2^2, \tag{7}$$

in which λ is a trade-off hyperparameter. This simple additional penalty, also considered in [18] in the context of transfer learning, can be interpreted as imposing a *prior*, which is learned from the supervised training set, on the network parameters; note the similarity of (7) to the formulation of other prior-based denoising methods.

With above two regularization methods, we fine-tune the supervised model $\tilde{\mathbf{w}}_{\text{sup}}$ by minimizing (7) and obtain the final weight parameters $\hat{\mathbf{w}}_{\texttt{FC-AIDE}}$. The denoising is then carried out by averaging the results obtained from applying $\hat{\mathbf{w}}_{\texttt{FC-AIDE}}$ in (6) to the 4 images in $\mathcal{A}(\mathbf{Z})$ separately. Note our data augmentation is different from the ordinary one in supervised learning, since we are *training* with the test data before testing. In Section 5.4, we analyze the effects of both regularization techniques on fine-tuning more in details.

5. Experimental results

5.1. Data and experimental setup

Training details For the supervised training, we exactly followed [38] and used 400 publicly available natural images of size 180×180 for building training dataset. We randomly sampled total 20,500 patches of size 120×120 from the images. Note the amount of information in our training data, in terms of the number of pixels, is roughly the same as that of DnCNN-S in [38] (204,800 patches of size 40×40), which uses 10 times more patches that are 9 times smaller than ours. Moreover, we used standard Gaussian noise augmentation for generating every mini-batch of clean-noisy patch pair for training of both σ-specific and the blindly trained models. Learning rates of 0.001 and 0.0003 were used for supervised training and fine-tuning, respectively, and Adam [15] optimizer was used. Learning rate decay was used only for the supervised training, and dropout or BatchNorm were not used. All experiments used Keras 2.2.0 with Tensorflow 1.8.0 and NVIDIA GTX1080TI.

Evaluation data We first used five benchmark datasets, Set5, Set12[38], BSD68[27] Urban100[13], and Manga109[24], to objectively compare the performance of FC-AIDE with other state-of-the-arts for Gaussian denoising. Among the benchmarks, Set12 and BSD68 contain general natural grayscale images of which characteristics are similar to that of the training set. In contrast, Set5 (visualized in the Supplementary Material), Urban100 (images with many self-similar patterns), and Manga109 (cartoon images) contain images that are quite different from the training data. We tested with five different noise levels, $\sigma = \{15, 25, 30, 50, 75\}$. Overall, we used the standard metrics, PSNR(dB) and SSIM, for evaluation.

In addition, we generated two additional datasets to evaluate and compare the adaptivities of the algorithms. Firstly, *Medical/Gaussian* is a set of 50 medical images (collected from the CT, MRI, and X-ray modalities) of size 400×400, corrupted by Gaussian noise with $\sigma = \{30, 50\}$. The images were obtained from the open repositories [34, 1, 5]. Clearly, their characteristics are radically different from natural images. Secondly, *BSD68/Laplacian* is generated by corrupting BSD68 by Laplacian noise with $\sigma = \{30, 50\}$. These datasets are built to test the adaptivity for the image and noise mismatches, respectively, since all the comparing CNN-based methods, including FC-AIDE, are supervised trained only on natural images with Gaussian noise.

Comparing methods The baselines we used were: BM3D [7], RED [22], Memnet [31], DnCNN-S and DnCNN-B [38], and N-AIDE [4]. For DnCNN and N-AIDE, we used the available source codes to reproduce *both* training (on the same supervised training data as FC-AIDE) and denoising, and for BM3D/RED/MemNet, we downloaded the models from the authors' website and carried out the denoising in our evaluation datasets. Thus, all the numbers in our tables are *fairly* comparable.

We denote $\texttt{FC-AIDE}_{\texttt{S+FT}}$ as our final model obtained after the supervised training and adaptive fine-tuning. For comparison purpose, we also report the results of the $\texttt{FC-AIDE}$ with subscripts $\texttt{S}$, $\texttt{B}$, and $\texttt{B+FT}$, which stand for the supervised-only model, the blindly trained supervised

Table 1. PSNR(dB)/SSIM on benchmarks with Gaussian noise. The best and the second best are denoted in red and blue, respectively.

Data	Noise	BM3D	RED	DnCNN_S	DnCNN_B	Memnet	N-AIDE_{S+FT}	FC-AIDE_S	FC-AIDE_{S+FT}	FC-AIDE_B	FC-AIDE_{B+FT}
Set5	σ=15	29.64/0.8983	-	30.22/0.9479	28.76/0.9364	-	30.23/0.9480	29.96/0.9461	**30.78/0.9518**	29.67/0.9453	**30.69/0.9514**
	σ=25	26.47/0.8983	-	27.01/0.9072	26.14/0.8948	-	27.05/0.9083	26.91/0.9083	**27.88/0.9191**	26.75/0.9070	**27.83/0.9182**
	σ=30	25.32/0.8764	25.14/0.8953	25.95/0.8882	25.15/0.8735	25.97/0.8909	26.01/0.8896	25.85/0.8890	**26.86/0.9038**	25.72/0.8882	**26.80/0.9030**
	σ=50	23.20/0.8139	23.02/0.8161	22.67/0.7969	22.58/0.7949	23.17/0.8205	23.08/0.8160	22.37/0.7992	**24.20/0.8482**	22.93/0.8117	**24.23/0.8475**
	σ=75	21.21/0.7409	-	20.47/0.6899	17.30/0.5437	-	20.95/0.7323	20.38/0.7091	**22.20/0.7889**	20.62/0.7176	**22.22/0.7857**
Set12	σ=15	32.15/0.8856	-	32.83/0.8964	32.50/0.8899	-	32.58/0.8918	32.71/0.8962	**32.99/0.9006**	32.48/0.8929	**32.91/0.8995**
	σ=25	29.67/0.8327	-	30.40/0.8513	30.15/0.8435	-	30.12/0.8420	30.32/0.8521	**30.57/0.8557**	30.16/0.8490	**30.51/0.8545**
	σ=30	28.74/0.8085	29.68/0.8378	29.53/0.8321	29.30/0.8233	29.62/**0.8374**	29.24/0.8214	29.47/0.8334	**29.74/0.8373**	29.33/0.8303	**29.63**/0.8353
	σ=50	26.55/0.7423	27.32/0.7748	27.16/0.7667	26.94/0.7528	**27.36/0.7791**	26.84/0.7492	27.16/0.7698	**27.42/0.7768**	27.04/0.7636	27.29/0.7693
	σ=75	24.68/0.6670	-	25.27/0.7001	17.64/0.2802	-	24.90/0.6749	25.37/0.7094	**25.61/0.7170**	24.93/0.6703	**25.39/0.6980**
BSD68	σ=15	31.07/0.8717	-	31.69/0.8869	31.40/0.8804	-	31.49/0.8825	31.67/0.8885	**31.78/0.8907**	31.53/0.8859	**31.71/0.8897**
	σ=25	28.56/0.8013	-	29.19/0.8202	28.99/0.8132	-	28.99/0.8137	29.20/0.8246	**29.31/0.8281**	29.11/0.8213	**29.26/0.8267**
	σ=30	27.74/0.7727	**28.45**/0.7987	28.36/0.7925	28.17/0.7847	28.42/0.7915	28.15/0.7842	28.38/0.7974	**28.49/0.8014**	28.30/0.7937	28.44/**0.7995**
	σ=50	25.60/0.6866	26.29/0.7124	26.19/0.7027	26.05/0.6934	**26.34/ 0.7190**	25.98/0.6911	26.27/0.7127	**26.38/0.7181**	26.18/0.7063	26.32/0.7132
	σ=75	24.19/0.6216	-	24.64/0.6240	17.91/0.2856	-	24.40/0.6101	24.77/0.6402	**24.89/0.6477**	24.41/0.6151	**24.75/0.6340**
Urban100	σ=15	31.61/0.9301	-	32.32/0.9375	31.75/0.9257	-	31.96/0.9340	31.98/0.9311	**32.85/0.9448**	31.54/0.9299	**32.65/0.9433**
	σ=25	28.76/0.8773	-	29.41/0.8884	29.04/0.8787	-	29.11/0.8861	29.15/0.8871	**30.05/0.9053**	28.91/0.8850	**29.91/0.9033**
	σ=30	27.71/0.8520	28.58/0.8743	28.38/0.8659	28.07/0.8556	28.57/0.8720	28.10/0.8622	28.16/0.8646	**29.06/0.8867**	27.99/0.8635	**28.91/0.8837**
	σ=50	25.22/0.7686	25.83/0.7946	25.66/0.7843	25.42/0.7732	26.00/0.8021	25.40/0.7767	25.55/0.7885	**26.42/0.8178**	25.46/0.7845	**26.23/0.8087**
	σ=75	23.20/0.6804	-	23.57/0.6973	18.35/0.4254	-	23.31/0.6843	23.61/0.7099	**24.42/0.7469**	23.28/0.6902	**24.11/0.7248**
Manga109	σ=15	32.02/0.9362	-	33.52/0.9489	33.01/0.9406	-	33.07/0.9450	33.24/0.9457	**33.86/0.9524**	32.83/0.9433	**33.70/0.9521**
	σ=25	29.00/0.8917	-	30.40/0.9121	30.15/0.9041	-	30.04/0.9071	30.24/0.9112	**30.80/0.9193**	30.02/0.9086	**30.72/0.9191**
	σ=30	27.91/0.8691	29.52/0.9011	29.33/0.8945	29.09/0.8851	29.55/0.9003	28.96/0.8880	29.18/0.8935	**29.75/0.9041**	29.02/0.8913	**29.65/0.9030**
	σ=50	25.24/0.7943	26.50/0.8358	26.38/0.8237	26.17/0.8146	26.64/0.8403	26.02/0.8160	26.28/0.8281	**26.79/0.8428**	26.19/0.8246	**26.66/0.8361**
	σ=75	23.20/0.7143	-	24.04/0.7394	18.82/0.4308	-	23.75/0.7355	24.06/0.7577	**24.54/0.7789**	23.76/0.7281	**24.33/0.7588**
Training data ratio		-	**x4.23**	x1	x1	**x4.23**	x1	x1	x1	x1	x1

model, and the blindly trained model fine-tuned with true σ, respectively. For N-AIDE, we also report the S+FT scheme, but the fine-tuning was done without any regularization methods. For the blind supervised models, DnCNN-B and FC-AIDE_B were all trained with Gaussian noise with $\sigma \in [0, 55]$. The stopping epochs for all our FC-AIDE models (both supervised and fine-tuned) as well as λ in (7) were selected from a separate validation set that is composed of 32 images from BSD [23]. All details regarding the experimental settings are given in the Supplementary Material.

5.2. Denoising results on the benchmark datasets

Table 1 shows the results on the 5 benchmark datasets, supervised training data size ratios, and the average denoising time per image for all comparing models. For RED and Memnet, we only have results for $\sigma = 30, 50$, since the models for other σ were not available. There are several observations that we can make. Firstly, we note FC-AIDE_{S+FT} outperforms all the comparing state-of-the-arts on most datasets in terms of PSNR/SSIM. Moreover, the gains of FC-AIDE_{S+FT} against the strongest baselines get significantly larger for the datasets that have the *image mismatches*, *i.e.*, Set5, Urban100, and Manga109. This is primarily due to the effectiveness of the adaptive fine-tuning step that significantly improves FC-AIDE_S . The additional results that highlight such adaptivity are also given in Section 5.3 and 5.4. Secondly, we note that FC-AIDE_{S+FT} uses much less supervised training data than RED and Memnet in terms of the number of pixels. Again, a more detailed analysis on the data efficiency of FC-AIDE_{S+FT} is given in Section 5.3. Thirdly, it is clear that FC-AIDE_{S+FT} is much better than N-AIDE_{S+FT}, which has the fully-connected structure and no regularizations for fine-tuning, confirming our contributions given in Section 4.1 and 4.2.

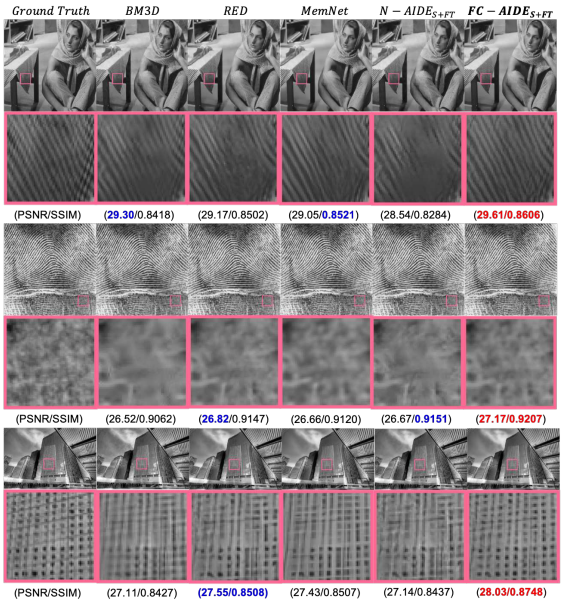

Figure 2. Denoising results ($\sigma = 30$) for *Barbara*, *F.print*, and *Image60* in Urban100.

Fourthly, we note FC-AIDE_{B+FT} also is quite strong, *i.e.*, gets very close to FC-AIDE_{S+FT} and mostly outperforms the other baselines with *matched* noise for supervised models. This result is interesting since it suggests maintaining just a single blindly trained supervised model, FC-AIDE_B , is sufficient as long as the true σ is available for the fine-tuning. Note also DnCNN-B fails dramatically for $\sigma = 75$, which is outside the noise levels that DnCNN-B is trained for, but FC-AIDE_{B+FT} corrects most of such *noise mismatch*. Finally, the denoising time of FC-AIDE_{S+FT} is larger than that of FC-AIDE_S, which is a cost to pay for

the adaptivity.

Figure 2 visualizes the denoising results for $\sigma = 30$, particularly for images with many self-similar patterns. A notable example is *Barbara*, in which other CNN baselines are worse than BM3D, but FC−AIDE$_{S+FT}$ significantly outperforms all others. Overall, we see that FC−AIDE$_{S+FT}$ performs very well on the images with self-similarities *without* any explicit non-local operations as in [19, 6].

5.3. Effects of adaptive fine-tuning

Here, we give additional results that highlight the three main scenarios in which the adaptivity of FC−AIDE$_{S+FT}$ gets particularly effective.

Data scarcity Figure 3 compares the PSNR of FC−AIDE$_{S+FT}$ with DnCNN-S on BSD68 ($\sigma = 25$) with varying training data size; *i.e.*, the horizontal axis represents the relative training data size compared to that used for training DnCNN-S in [38], in terms of the number of pixels. The performance of N-AIDE$_S$ and N-AIDE$_{S+FT}$ are also shown for comparison purpose. From the figure, we observe that FC−AIDE$_{S+FT}$ surpasses DnCNN-S (100%) with using only 30% of the training data due to the two facts; the base supervised model FC−AIDE$_S$ is more data-efficient (*i.e.*, FC−AIDE$_S$ with 30% data outperforms DnCNN-S (30%)), and the fine-tuning gives another 0.1dB PSNR boost.

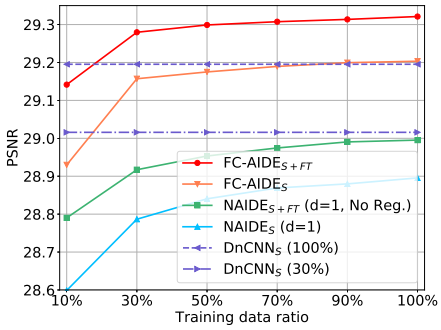

Figure 3. Data efficiency over DnCNN[38] for BSD68 ($\sigma = 25$).

Image mismatch Table 2 gives denoising results on *Medical/Gaussian*, which consists of 50 medical images with radically different characteristics compared to the natural images in the supervised training set of RED, Memnet, and FC−AIDE$_S$. From the table, we again see that FC−AIDE$_{S+FT}$ outperforms RED and Memnet despite FC−AIDE$_S$ being slightly worse than them, thanks to the adaptivity of fine-tuning. Moreover, we consider a scenario in which there is only a small number of *matched* supervised training data available; *i.e.*, FC−AIDE$_{S\,(M)}$ in Table 2 is a supervised model trained with only 10 medical images. In this case, we observe that FC−AIDE$_{S\,(M)}$ is even worse than above three *mismatched* supervised models, due to the small training data size. However, via fine-tuning, we observe FC−AIDE$_{S\,(M)\,+FT}$ surpasses all other models and achieves the best PSNR, which shows the effectiveness of the adaptivity for fixing the image mismatches.

Table 2. PSNR(dB)/SSIM on *Medical/Gaussian*. Color as before.

Noise	RED	Memnet	N-AIDE$_{S+FT}$	FC−AIDE$_S$	FC−AIDE$_{S+FT}$	FC−AIDE$_{S\,(M)}$	FC−AIDE$_{S\,(M)\,+FT}$
$\sigma = 30$	35.12/0.9005	35.02/0.8986	34.70/0.8920	35.01/0.8980	**35.26/0.9030**	34.96/0.8993	**35.37/0.9050**
$\sigma = 50$	32.78/0.8660	32.87/0.8691	32.23/0.8499	32.74/0.8641	**32.99/0.8703**	32.56/0.8628	**33.06/0.8727**

From Table 1 and Figure 3, one may think the gain of FC−AIDE$_{S+FT}$ over FC−AIDE$_S$ is relatively small for BSD68 (*e.g.*, 0.1dB on average for $\sigma = 25$). We stress, however, that this is due to the similarity between the training data and BSD68. That is, Figure 4 shows the top 4 images in BSD68 ($\sigma = 25$) that FC−AIDE$_{S+FT}$ had the most improvement over FC−AIDE$_S$; the improvement for each image was 0.53dB, 0.49dB, 0.38dB, and 0.29dB, respectively, which are much higher than the average. The pixels that had the most MSE improvements are shown as yellow pixels in the second row. We clearly observe that these images are with many self-similar patterns and see that FC−AIDE$_{S+FT}$ gets particularly strong primarily at pixels with those patterns. Images with specific self-similar patterns can be considered as another form of *image mismatch*, and we confirm the effectiveness of our fine-tuning.

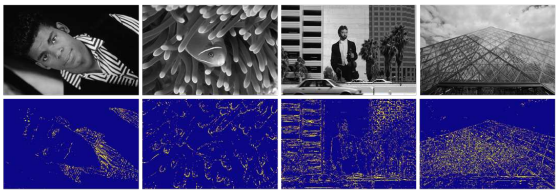

Figure 4. Row 1: Top 4 images in BSD68 ($\sigma = 25$) that had the most PSNR improvements by FC−AIDE$_{S+FT}$ over FC−AIDE$_S$ Row 2: The pixels that had most improvements.

Noise mismatch Table 3 shows the denoising results on *BSD68/Laplacian*. Since all the supervised models in the table are trained with Gaussian noise, the setting corresponds to the *noise mismatch* case. As ideal upper bounds, we also report the performance of FC−AIDE$_{S\,(L)}$ and FC−AIDE$_{S\,(L)\,+FT}$, which stand for the supervised model trained with Laplacian noise-corrupted data and its fine-tuned model, respectively. We can see that among models using the mismatched supervised models, FC−AIDE$_{S+FT}$ again achieves the best denoising performance followed by FC−AIDE$_{B+FT}$, without any information on the noise distribution other that σ. Moreover, we observe the PSNR gap between FC−AIDE$_S$ and FC−AIDE$_{S\,(L)}$ are much reduced after fine-tuning, and the gaps between FC−AIDE$_{S+FT}$ and the other baselines widened compared to those in Table 1.

5.4. Ablation study and analyses

Here, we give more detailed analyses justifying our modeling choices given in Section 4.1 and 4.2.

Ablation study on model architecture Figure 5 shows several ablation studies on BSD68 ($\sigma = 25$) with varying

Table 3. PSNR(dB)/SSIM on BSD68 with Laplacian noise. The best and the second best are denoted in red and blue, respectively.

Noise	BM3D	RED	DnCNN-S	DnCNN-B	Memnet	N-AIDE$_{S+FT}$	FC-AIDE$_{S}$	FC-AIDE$_{S+FT}$	FC-AIDE$_{B}$	FC-AIDE$_{B+FT}$	FC-AIDE$_{S\,(L)}$	FC-AIDE$_{S\,(L)\,+FT}$
σ=30	27.48/0.7564	28.18/0.7887	28.01/0.7783	27.69/0.7650	28.26/0.7916	28.08/0.7797	28.28/0.7917	**28.42/0.7983**	28.12/0.7886	**28.41/0.7979**	28.63/0.8076	**28.70/0.8090**
σ=50	25.52/0.6669	26.10/0.7030	25.90/0.6878	25.68/0.6769	26.13/0.7098	25.91/0.6858	26.17/0.7067	**26.31/0.7123**	25.92/0.6954	**26.27/0.7077**	26.64/0.7293	**26.70/0.7317**

model architectures. Firstly, Figure 5(a) shows the PSNR

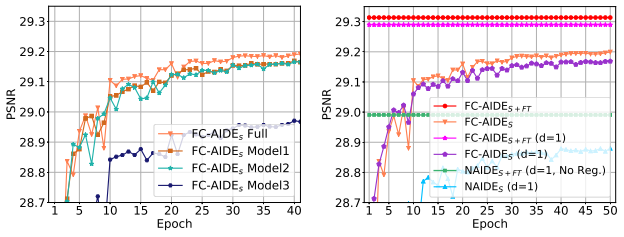

(a) Model architecture variations (b) Improvements over N-AIDE [4].

Figure 5. Ablation studies for FC-AIDE on BSD68 ($\sigma = 25$).

of FC-AIDE$_S$ with several varying architectures with respect to the training epochs. "Full" stands for the model architecture in Figure 1(a), "Model 1" is without the ResNet Modules in Block 2, "Model 2" is without the ResNet Module in Block 3, and "Model 3" is without both ResNet Modules. The figure shows the ResNet Modules in Figure 1(a) are all critical in our model. Secondly, Figure 5(b) compares FC-AIDE$_{S+FT}$ to its $d = 1$ version as well as to N-AIDE [4]. We clearly observe the benefit of our QED architecture over the fully-connected architecture, since the supervised-only FC-AIDE$_S$ ($d = 1$) significantly outperforms both N-AIDE$_S$ and N-AIDE$_{S+FT}$. Moreover, we observe the quadratic mappings for FC-AIDE$_{S+FT}$ also are beneficial in further improving the PSNR.

Table 4. PSNR(dB) on BSD68 ($\sigma = 25$).

Data\Alg.	FC-AIDE$_S$	FC-AIDE$_{S+FT}$	NO-QED$_S$	NO-QED$_{S+FT}$	FC-AIDE$_{FT}$
BSD68	29.20	**29.31**	29.16	21.93	23.76

In Table 4, we justify our QED architecture, which satisfies the conditional independence constraint mentioned in Section 4.1, by comparing with a CNN that learns the same polynomial mapping (2) with vanilla convolution filters, which violates the constraint. Such model, dubbed as NO-QED, had the same number of layers and receptive field as those of FC-AIDE. We observe that while the supervised model, NO-QED$_S$ gets quite close to FC-AIDE$_S$, the fine-tuned model NO-QED$_{S+FT}$ dramatically deteriorates. This shows the conditional independence constraint is indispensable for the fine-tuning and justifies our QED architecture. Moreover, Table 4 also shows the performance of FC-AIDE$_{FT}$, which only carries out fine-tuning with randomly initialized parameters. The result clearly shows the importance of supervised training for FC-AIDE.

Effect of regularization Figure 6 shows the effect of each regularization method in Section 4.2 on BSD68 ($\sigma = 25$). Firstly, Figure 6(a) compares the PSNR of FC-AIDE$_{S+FT}$ with and without the data augmentation. We clearly observe that the data augmentation gives a further boost of PSNR compared to just using single $\mathbf{Z}$. Secondly, Figure 6(b) shows MSE (orange) and estimated loss (blue) during fine-tuning with and without ℓ_2-SP. We can clearly observe that when there is no ℓ_2-SP, the trends of MSE and the estimated loss diverges (*i.e.*, *overfitting* occurs), but with ℓ_2-SP, minimizing the estimated loss generalizes well to minimizing the MSE with robustness.

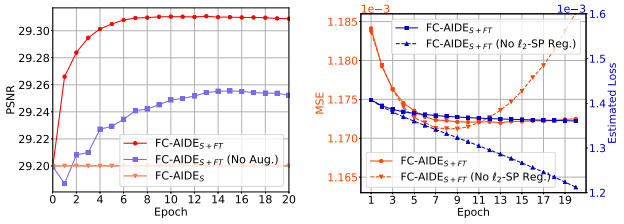

(a) Data augmentation (b) ℓ_2-SP

Figure 6. Effects of regularization methods for BSD68 ($\sigma = 25$).

Visualization of polynomial mapping Figure 7 visualizes the pixelwise polynomial coefficients $\{a_{m,i}\}_{m=0}^{2}$ learned for *Image13* of BSD68 ($\sigma = 25$). We note the coefficient values for the higher order terms are relatively small compared to $\{a_{0,i}\}$'s. But, we observe they become more salient particularly for the high frequency parts of the image, *i.e.*, the edges. The effects of the polynomial coefficients on denoising is given in the Supplementary Material.

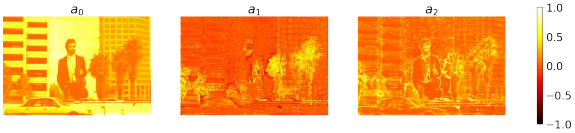

Figure 7. Visualization of a_0, a_1 and a_2 for *Image13* in BSD68.

6. Conclusion

We proposed FC-AIDE that can *both* supervised-train and adaptively fine-tune the CNN-based pixelwise denoising mappings. While surpassing the strong recent baselines, we showed that the adaptivity of our method can resolve various mismatch as well as data scarce scenarios commonly encountered in practice. Possible future research directions include extending our method to other general image restoration problems, *e.g.*, image super-resolution, beyond denoising and devise a full blind denoising method that can also estimate the noise σ.

Acknowledgement

This work is supported in part by the ICT R&D Program [2016-0-00563], AI Graduate School Support Program [2019-0-00421], and ITRC Support Program [2019-2018-0-01798] of MSIT / IITP of the Korean government.

References

[1] National cancer institute clinical proteomic tumor analysis consortium (cptac). https://doi.org/10.7937/k9/tcia.2018.oblamn27.

[2] A. Buades, B. Coll, and J. M. Morel. A review of image denoising algorithms, with a new one. *SIAM Journal on Multiscale Modeling and Simulation: A SIAM Interdisciplinary Journal*, 2005.

[3] H. Burger, C. Schuler, and S. Harmeling. Image denoising: Can plain neural networks compete with BM3D? In *Computer Vision and Pattern Recognition (CVPR)*, 2012.

[4] Sungmin Cha and Taesup Moon. Neural adaptive image denoiser. In *IEEE ICASSP*, 2018.

[5] Jun Cheng. Brain tumor dataset, 2017.

[6] Cristovao Cruz, Alessandro Foi, Vladimir Katkovnik, and Karen Egiazarian. Nonlocality-reinforced convolutional neural networks for image denoising. *https://arxiv.org/pdf/1803.02112.pdf*, 2018.

[7] K. Dabov, A. Foi, V. Katkovnik, and K. Egiazarian. Image denoising by sparse 3-d transform-domain collaborative filtering. *IEEE Trans. Image Processing*, 16(8):2080–2095, 2007.

[8] D. Donoho and I. Johnstone. Adapting to unknown smoothness via wavelet shrinkage. *Journal of American Statistical Association*, 90(432):1200–1224, 1995.

[9] M. Elad and M. Aharon. Image denoising via sparse and redundant representations over learned dictionaries. *IEEE Trans. Image Processing*, 54(12):3736–3745, 2006.

[10] Y. Eldar. Rethinking biased estimation: Improving maximum likelihood and the Cramer-Rao bound. *Foundations and Trends in Signal Processing*, 1(4):305–449, 2008.

[11] S. Gu, L. Zhang, W. Zuo, and X. Feng. Weighted nuclear norm minimization with applicaitons to image denoising. In *Computer Vision and Pattern Recognition (CVPR)*, 2014.

[12] Kaiming He, Xiangyu Zhang, Shaoqing Ren, and Jian Sun. Delving deep into rectifiers: Surpassing human-level performance on imagenet classification. In *CVPR*, 2015.

[13] J-B Huang, A. Singh, and N. Ahuja. Single image super-resolution from transformed self-exemplars. In *CVPR*, 2015.

[14] V. Jain and H.S. Seung. Natural image denoising with convolutional networks. In *NIPS*, 2008.

[15] D. Kingma and J. Ba. Adam: A method for stochastic optimization. In *International Conference on Learning Representations (ICLR)*, 2015.

[16] Stamatios Lefkimmiatis. Universal denoising networks: A novel CNN architecture for image denoising. In *CVPR*, 2018.

[17] Jaakko Lehtinen, Jacob Munkberg, Jon Hasselgren, Samuli Laine, Tero Karras, Miika Aittala, and Timo Aila. Noise2Noise: Learning image restoration without clean data. In *ICML*, 2018.

[18] X. Li, Y. Grandvalet, and F. Davoine. Explicit inductive bias for transfer learning with convolutional networks. In *ICML*, 2018.

[19] Ding Liu, Bihan Wen, Yuchen Fan, Chen C. Loy, and Thomas S. Huang. Non-local recurrent network for image restoration. In *NIPS*, 2018.

[20] S. Lunz, O. Öktem, and C.-B. Schönlieb. Adversarial regularizers in inverse problems. In *NIPS*, 2018.

[21] J. Mairal, F. Bach, J. Ponce, G. Sapiro, and A. Zisserman. Non-local sparse models for image restoration. In *International Conference on Computer Vision (ICCV)*, 2009.

[22] X. Mao, C. Shen, and Y-B. Yang. Image restoration using very deep convolutional encoder-decoder networks with symmetric skip connections. *Neural Information Processing Systems (NIPS)*, 2016.

[23] D. Martin, C. Fowlkes, D. Tal, and J. Malik. A database of human segmented natural images and its application to evaluating segmentation algorithms and measuring ecological statistics. In *International Conference on Computer Vision (ICCV)*, 2001.

[24] Y. Matsui, K. Ito, Y. Aramaki, A. Fujimoto, T. Ogawa, T. Yamasaki, and K. Aizawa. Sketch-based manga retrieval using Manga109 dataset. *Multimed. Tools Appl.*, 76(21811), 2017.

[25] T. Moon, S. Min, B. Lee, and S. Yoon. Neural universal discrete denosier. In *Neural Information Processing Systems (NIPS)*, 2016.

[26] Giovanni Motta, Erik Ordentlich, Ignacio Ramirez, Gadiel Seroussi, and Marcelo J. Weinberger. The iDUDE framework for grayscale image denoising. *IEEE Trans. Image Processing*, 20:1–21, 2011.

[27] S. Roth and M.J Black. Field of experts. *International Journal of Computer Vision*, 82(2):205–229, 2009.

[28] K. Sivaramakrishnan and T. Weissman. Universal denoising of discrete-time continuous-amplitude signals. *IEEE Trans. Inform. Theory*, 54(12):5632–5660, 2008.

[29] Shakarim Soltanayev and Se Young Chun. Training deep learning based denoisers without ground truth data. In *NIPS*, 2018.

[30] C. Stein. Estimation of the mean of a multivariate normal distribution. *The Annals of Statistics*, 9(6):1135–1151, 1981.

[31] Ying Tai, Jian Yang, Xiaoming Liu, and Chunyan Xu. Memnet: A persistent memory network for image restoration. In *ICCV*, 2017.

[32] Dmitry Ulyanov, Andrea Vedaldi, and Victor Lempitsky. Deep image prior. In *CVPR*, 2018.

[33] Aäron van den Oord, Nal Kalchbrenner, Oriol Vinyals, Lasse Esleholt, Alex Graves, and Koray Kavukcuoglu. Conditional image generation with PixelCNN decoders. In *NIPS*, 2016.

[34] Xiaosong Wang, Yifan Peng, Le Lu, Zhiyong Lu, MohammadhadiBagheri, and Ronald M. Summers. Chestx-ray8: Hospital-scale chest x-ray database and benchmarks on weakly-supervised classification and localization of common thorax diseases. In *CVPR*, 2017.

[35] T. Weissman, E. Ordentlich, G. Seroussi, S. Verdu, and M. Weinberger. Universal discrete denoising: Known channel. *IEEE Trans. Inform. Theory*, 51(1):5–28, 2005.

[36] J. Xie, L. Xu, and E. Chen. Image denoising and inpainting with deep neural networks. In *Neural Information Processing Systems (NIPS)*, 2012.

[37] R.A. Yeh, T. Y. Lim, C. Chen, A. G. Schwing, M. Hasegawa-Johnson, and M. N. Do. Image restoration with deep generative models. In *ICASSP*, 2018.

[38] K. Zhang, W. Zuo, Y. Chen, D. Meng, and L. Zhang. Beyond a gaussian denoiser: Residual learning of deep cnn for image denoising. *IEEE Trans. Image Processing*, 26(7):3142 – 3155, 2017.

[39] D. Zoran and Y. Weiss. From learning models of natural image patches to whole image restoration. *International Conference on Computer Vision (ICCV)*, 2011.